Proceedings of the ASME 2010 3rd Joint US-European Fluids Engineering Summer Meeting and 8th International Conference on Nanochannels, Microchannels, and Minichannels
FEDSM-ICNMM2010
August 1-5, 2010, Montreal, Canada

FEDSM-ICNMM2010-31130

COMPUTATIONAL MODELING OF THERMAL ENERGY STORAGE IN ROCK BEDS

Tihomir G. Sivov
Heat Transfer Laboratory
Department of Mechanical Engineering, McGill University
Montreal, Quebec, Canada

Raul Palacios-Gamez
Heat Transfer Laboratory
Department of Mechanical Engineering, McGill University
Montreal, Quebec, Canada

B. Rabi Baliga
Heat Transfer Laboratory
Department of Mechanical Engineering, McGill University
Montreal, Quebec, Canada

ABSTRACT

Thermal energy storage (TES) systems are commonly employed for enhancing the efficiency of commercial and residential heating and cooling systems, by matching thermal energy supply and demand during summer-winter, day-night, and peak-off-peak periods. TES in these systems is usually achieved by changing the temperature of materials (sensible systems) and/or inducing solid-liquid phase change (latent heat systems). Such systems are also categorized as seasonal (long-term) and diurnal (short-term). In this work, the focus is on sensible diurnal TES systems consisting of rock beds, with air as the working fluid. They are relatively simple, easy to construct, inexpensive, and quite effective for many solar energy and building engineering applications. Numerous publications on rock-bed TES systems are available, but there is an urgent need for efficient computational methods for designing and optimizing them. The contributions of this work are the following: proposal of cost-effective mathematical models of fluid flow and heat transfer in rock beds; adaptation of a finite volume method (FVM) for the solution of this model; applications of this FVM to two test problems (with analytical solutions) and one demonstration problem; proposal of suitable thermofluid performance evaluation criteria for the rock-bed TES systems of interest; and presentation and discussions of the results.

INTRODUCTION

Examples of thermal energy storage (TES) systems date back to ancient civilizations and include the following: caves for living and storage of foods; use of winter ice for summer cooling and preservation of foods; adobe and other thick-walled huts; and igloos. Over the last 60 years, TES units have been employed extensively for enhancing the efficiency of commercial and residential heating and cooling systems, by matching thermal energy supply and demand during summer-winter, day-night, and peak-off-peak periods. TES devices have also been used for passive thermal control of electronics systems, spacecrafts in earth orbits, and transportation systems.

In the aforementioned systems, TES is usually achieved by changing the temperature of materials (sensible systems) and/or by inducing solid-liquid phase change (latent heat systems). Commonly used media and systems for sensible TES include the following [Paksoy (2007)]: water contained in suitable tanks; bricks, stone, concrete, and metals particles in appropriate containers; Trombe walls; artificial rock beds in above-ground or underground containers; solar ponds; underground aquifers; and underground boreholes. In solid-liquid phase-change TES systems, ice-water, paraffins, and salts are commonly used [Zalba et al. (2003); Paksoy (2007); Mehling and Cabeza (2008)]. TES systems are also categorized as seasonal (or long-term) and diurnal (or short-term): the thermal energy charging (storage) and discharging (harvesting) periods in seasonal and diurnal TES systems are typically of the order of half-year and half-day, respectively. Detailed discussions and reviews of the aforementioned TES systems are available in the works of Dincer and Rosen (2002), and Paksoy (2007).

In this work, the focus is on sensible diurnal TES systems consisting of rock beds, with air as the working fluid. Such systems are relatively simple, easy to construct, inexpensive, and quite effective for many solar energy and building engineering applications. In particular, attention here is devoted to mathematical models and computer simulations of air flows and unsteady forced convection heat transfer in the aforementioned TES systems. The commonly used media in rock-bed TES units are granite, limestone, marble, and sandstone, typically in the form of essentially uniform-sized pebbles of almost spherical shape. The development and implementation of cost-effective computational tools for the design of such TES units would have significant socio-

economic and environmental benefits. These potential benefits constitute the main motivation for the work described in this paper.

In the published literature, there are numerous publications on rock-bed TES systems: comprehensive reviews are available in Dincer and Rosen (2002), and Paksoy (2007). However, there is an urgent need for efficient computational methods for designing and optimizing these TES systems, and the goal here is to fulfill at least a part of this need. The specific contributions of this work are the following: proposal of cost-effective mathematical models of fluid flow and heat transfer in rock beds, based mainly on the works of Darcy (1856), Brinkman (1947), Scheidegger (1974), Wakao and Kaguei (1982), Dullien (1992), Kaviany (1995), Whitaker (1996, 1999), Nield and Bejan (1999), and Alzami and Vafai (2000); adaptation of a finite volume method (FVM) [Patankar (1980); Baliga and Atabaki (2007)] for the solution of these models; testing of this FVM using analytical solutions based on the works of Schuman (1929), Riaz (1977), and Haji-Sheikh (2006); applications of this FVM to a demonstration problem; proposal of suitable thermofluid performance evaluation criteria for the rock-bed TES systems of interest, borrowing some ideas from Rosen (1992), and Dincer and Rosen (2002); and presentation and discussions of the results.

NOMENCLATURE

$a_C, a_E, a_W, a_N, a_S, b$	coefficients in the discretized equations (FVM)
a_{sf}	specific surface area [m^{-1}]
C_f	Frochheimer coefficient
c_p	specific heat at constant pressure [J/(kg.K)]
COP	coefficient of performance
d_p	mean effective particle diameter [m]
E	thermal energy [J]
g	acceleration due to gravity [m/s^2]
h	convection heat transfer coefficient [$W/(m^2.K)$]
H	half-height of rock bed [m]
k	thermal conductivity [W/(m.K)]
K	permeability [m^2]
L	length of rock bed [m]
$\dot{m}$	fluid mass flow rate [kg/s]
Nu	Nusselt number
p	intrinsic-phase-average static pressure [N/m^2]
P	intrinsic-phase-average reduced pressure [N/m^2]
Pr	Prandtl number
Re	Reynolds number
S	volumetric (per unit volume) source term
T	intrinsic-phase-average temperature [^oC]
V	volume of the rock bed [m^3]
$\vec{v}$, u, v	Darcy (or superficial) velocity vector and its x- and y-direction components [m/s]
W	depth of the rock bed [m]
x, y, z	Cartesian coordinates [m]

Greek symbols

α	thermal diffusivity [m^2/s]
ε	porosity
ϕ	general specific (per unit mass) scalar dependent variable
Γ_ϕ	diffusion coefficient associated with ϕ
η	efficiency coefficient
μ	dynamic viscosity [kg/(m.s)]
ν	kinematic viscosity [m^2/s]
ρ	mass density [kg/m^3]

Subscripts

ch	charging mode
disch	discharging mode
eff	effective
f	fluid phase
in	inlet plane of the rock bed
ini	initial conditions
s	solid phase
sf	solid-fluid interface

Superscripts

o	old or previous value in time
P	intrinsic-phase-average reduced pressure
T_f	intrinsic-phase-average temperature of fluid phase
T_s	intrinsic-phase-average temperature of solid phase
u	*x*-direction Darcy velocity component
v	y-direction Darcy velocity component

MATHEMATICAL MODELS

Cost-effective mathematical models of fluid flow and heat transfer in the rock-bed TES systems considered in this work are presented in this section.

Problem Statement, Assumptions, and Volume-Average Approach: A rock-bed TES system akin to those of interest in this work is schematically presented in Figure 1, along with an expanded view of a representative elementary volume (r.e.v.) within this bed, and related notation. The main TES component of this system consists of a close-packed bed of rocks, which are assumed to be essential spherical in shape and uniform in size. Hot or cold air is forced at a constant mass flow rate, $\dot{m}$, through this bed during the thermal energy storage (charging) or harvesting (discharging) operations, respectively. The rock bed is contained between two parallel, solid, impermeable plates. The length of the rock bed in the main air flow direction is L; the perpendicular distance between the inner surfaces of the parallel plates is $2H$; and the width, W, of the rock bed in the direction perpendicular to the plane shown in Figure 1 is large compared to both L and $2H$.

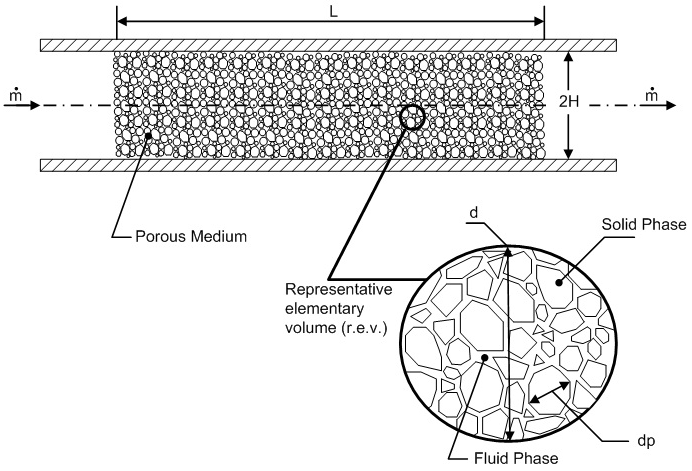

Figure 1: Schematic representation of a rock-bed TES system, a representative elementary volume, and related notation.

Attention in this work is limited to problems for which the following assumptions apply: the rock bed is a homogeneous and isotropic porous medium, with constant porosity and permeability; the rock bed is fully saturated with air, which behaves as a Newtonian fluid; the thermophysical properties of the fluid (ρ_f, μ_f, k_f, and $c_{p,f}$) and the rocks (ρ_s, k_s, and $c_{p,s}$) remain essentially constant, at suitable average values; and laminar fluid flow and forced convection heat transfer inside the rock bed.

One approach to the modeling of the rock-bed TES systems considered here is called the complete local or microscopic scale description, in which the Newtonian fluid flow in the pores of the porous medium, and the heat transfer in the fluid and the solid phases, are modeled using the continuity, Navier-Stokes, and energy equations, along with the no-slip, impermeability, continuity of temperature, and continuity of heat flux boundary conditions at all fluid-solid interfaces [Whitaker (1996, 1999); Scheidegger (1974); White (1991); Nield and Bejan (1992); Kaviany (1995)]. This approach is exact, but with currently available computers, it is far too time-consuming for the simulation of most problems of practical interest. Furthermore, exact geometrical descriptions at this scale are also impractical for rock-bed TES systems, due to their high *local* heterogeneity [Dullien (1992)].

The commonly used way around the above-mentioned difficulty with the complete local description is to use a volume-average approach to obtain a practically viable set of governing equations. The governing equations of the complete local description of the fluid flow and heat transfer in the porous medium are formally integrated over a representative elementary volume (r. e. v.), akin to that depicted in Figure 1. The length scale, d, of the r. e. v. is presumed to be much larger than the effective particle diameter, d_p, but much smaller than the global scale of the domain under consideration, or $d_p << d << L$ [Whitaker (1999)]. Two types of average values are introduced for any physical variable ψ: the phase-average (also referred to as the superficial average) value denoted by $\langle\psi\rangle$; and the intrinsic-phase-average (also referred to simply as the intrinsic-average) value denoted by $\langle\psi\rangle^f$. These average values are defined as follows:

$$\langle\psi\rangle \triangleq \frac{1}{V}\int_{V_f}\psi dV \;\;;\;\; \langle\psi\rangle^f \triangleq \frac{1}{V_f}\int_{V_f}\psi dV \tag{1}$$

In Eq. (1), V is the representative elementary volume and V_f represents the volume of the fluid phase contained within V. These two average values are related through the porosity, ε, by the Dupuit-Forchheimer relation [Nield and Bejan (1992)]: $\langle\psi\rangle = \varepsilon\langle\psi\rangle^f$. In this paper, for simplicity in the notation and convenience in the presentation, the phase-average velocity vector is denoted by $\vec{v}$, and its components in the Cartesian coordinate directions *x*, *y*, and *z* are denoted by *u*, *v*, and *w*, respectively; and the *intrinsic-phase-average* reduced pressure, $\langle P\rangle^f$, is indicated simply as *P*, where $P = p + \rho g y$, with *p* denoting the static pressure and *g* the acceleration due to gravity (directed in the negative *y* direction). It should be noted that in the published literature, the phase-average velocity, $\vec{v}$, is also referred to as the seepage, filtration, superficial, and Darcy velocity [Nield and Bejan (1992)].

Continuity Equation: In the context of the above-mentioned assumptions and notation, the continuity equation written in terms of the phase-average velocity vector, $\vec{v}$, and the mass density of the fluid, ρ_f, can be cast in the following form [Nield and Bejan (1992)]:

$$\vec{\nabla}.(\rho_f\vec{v}) = 0 \tag{2}$$

Momentum Equations: With regard to the conservation of momentum of the air flowing through the rock bed, both inertial and viscous effects are considered, and the so-called Darcy-Brinkman-Forchheimer equations [Nield and Bejan (1992)] are used. Several variants of these equations appear in the published literature, as discussed, for example, by Alazmi and Vafai (2000). Here, following the pioneering work of Vafai and Tien (1981) and the rigorous derivations provided by Whitaker (1996, 1999), the following form of these equations is employed:

$$\rho_f\left[\frac{1}{\varepsilon}\frac{\partial\vec{v}}{\partial t} + \frac{1}{\varepsilon^2}\left(\vec{v}\cdot\vec{\nabla}\right)\vec{v}\right] = -\vec{\nabla}P + \frac{\mu_f}{\varepsilon}\nabla^2\vec{v} - \frac{\mu_f}{K}\vec{v} - \frac{C_F\rho_f}{\sqrt{K}}|\vec{v}|\vec{v} \tag{3}$$

In Eq. (3), ρ_f is the density of the fluid; *P* is the intrinsic-phase-average reduced pressure; μ_f is the dynamic viscosity of the fluid; ε and *K* are the porosity and the permeability of the porous medium, respectively; and C_F is a dimensionless form-drag coefficient that is often referred to as the

Forchheimer coefficient [Whitaker (1996, 1999)]. The permeability, *K*, is independent of the nature of the fluid but it depends on the geometry of the porous medium, as discussed, for example, in the works of Dullien (1979), Nield and Bejan (1992), and Kaviany (1995). The Forchheimer coefficient, C_F, also depends on the geometry of the porous medium: related discussions are available in Nield and Bejan (1992), Kaviany (1995) and Alazmi and Vafai (2000). It should be noted that in the term $(\mu_f / \varepsilon)\nabla^2 \vec{v}$, a Brinkman viscosity, μ_B, or an effective viscosity, μ_{eff}, is sometimes used instead of (μ_f / ε); however, the theoretical developments of Whitaker (1999) show that this is unnecessary. Following the recommendations in Nield and Bejan (1992), the permeability, K, and the Forchheimer coefficient, C_F, in Eq. (3) are related to the porosity, ε, and the effective particle diameter, d_P, as follows:

$$\varepsilon = \frac{V_f}{V_f + V_s} = \frac{V_f}{V} \;;\; K = \left(\frac{\varepsilon^3}{180(1-\varepsilon)^2} \right) d_p^2 \;;\; C_F = \frac{1.75}{\sqrt{150\varepsilon^3}} \quad (4)$$

The above-mentioned relation for the permeability, *K*, is often referred to as the Carman-Kozeny equation.

With regard to the use of Eqs. (3) and (4) for thermofluid designs of rock-bed TES systems, it is important to note the following cost-effective simplification, the validity of which was established in this work: preliminary computations based on the full forms of Eqs. (3) and (4) indicated that for the flows of air in the TES systems of interest, if the inlet and outlet boundary conditions on the superficial velocity are maintained steady, then a steady-state distribution of $\vec{v}$ is achieved very rapidly after the start of the charging or discharging operations, compared to the overall time durations of these operations. Thus, the unsteady term, $(\rho_f / \varepsilon)\partial \vec{v} / \partial t$, in Eq. (3) can be dropped, and major reductions in the CPU times can be achieved in the computer simulations.

Energy Equations: Two different volume-average approaches to the modeling of convection heat transfer in porous media are available in the literature: in one, which leads to the single-phase or one-temperature model, the averaging is done over a representative elementary volume (r.e.v.) containing both the fluid and solid phases, and it is assumed that the temperatures of these two phases are essentially in equilibrium locally; in the other approach, which results in the two-phase or two-temperature model, intrinsic-phase-averaging is done for both the fluid and solid phases, resulting in two separate energy equations and temperature distributions, one for each individual phase. For computer simulations of the charging and discharging operations of the rock-bed TES systems considered in this work, it is necessary to use the two-phase or two-temperature model: thus, it is the one that is described in this section. However, one major simplification is invoked: it is assumed that thermal dispersion effects, caused by enhanced mixing of the working fluid in the tortuous flow paths and the wakes behind the particles that constitute the porous bed, are negligible. This assumption is valid when the Reynolds number based on the superficial velocity of the fluid flowing through the porous bed and the particle diameter is relatively low. If necessary, the thermal dispersion effects could be included using the recommendations available in the works of Nield and Bejan (1992) and Kaviany (1995).

In the context of the aforementioned restrictions and assumptions, the two-temperature model adopted in this work consists of the following two intrinsic-phase-average energy equations, one for the solid phase and the other for the fluid phase [Nield and Bejan (1992); Kaviany (1995)]:

Solid-phase energy equation:

$$(1-\varepsilon)(\rho c_P)_s \frac{\partial T_s}{\partial t} = \vec{\nabla} \cdot \left(k_{s,eff} \vec{\nabla} T_s \right) + h_{sf} a_{sf} \left(T_f - T_s \right) \quad (5)$$

Fluid-phase energy equation:

$$\varepsilon (\rho c_P)_f \frac{\partial T_f}{\partial t} + (\rho c_P)_f \vec{v} \cdot \vec{\nabla} T_f = \vec{\nabla} \cdot \left(k_{f,eff} \vec{\nabla} T_f \right) + h_{sf} a_{sf} \left(T_s - T_f \right) \quad (6)$$

In these equations, T_s and T_f are simplified notations for the intrinsic-phase-average temperatures, $\langle T_s \rangle^s$ and $\langle T_f \rangle^f$, of the solid and fluid phases, respectively; $k_{s,eff}$ and $k_{f,eff}$ are the effective thermal conductivities of the solid and fluid phases, respectively; h_{sf} is an average heat transfer coefficient at the interface between the solid particles and the fluid; and a_{sf} is the specific solid-fluid interfacial area (that is, the total area of the solid-fluid interface per unit volume of the rock bed).

Following the recommendations of Nield and Bejan (1992), and Kaviany (1995), the following expressions are used for $k_{s,eff}$ and $k_{f,eff}$:

$$k_{s,eff} = (1-\varepsilon) k_s \;;\; k_{f,eff} = \varepsilon k_f \quad (7)$$

The interfacial convection heat transfer coefficient, h_{sf}, is calculated using an empirical correlation proposed by Wakao and Kaguei (1982). It is based on the so-called particle-to-fluid Nusselt number, Nu_{sf}, and is valid for values of the Reynolds number based on the particle diameter in the range 15 to 8500. This correlation is the following:

$$Nu_{sf} \triangleq \frac{h_{sf} d_p}{k_f} = 2 + 1.1 \mathrm{Pr}^{1/3} \mathrm{Re}_{d_p}^{0.6} \quad (8)$$

In this equation, Re_{d_p} is the local particle Reynolds number, and Pr is the Prandtl number of the fluid:

$$\mathrm{Re}_{d_p} \triangleq \frac{\rho_f \, | \vec{v} \, | \, d_p}{\mu_f} \;;\; \mathrm{Pr} = \frac{\mu_f c_{p,f}}{k_f} \quad (9)$$

For close-packed beds of spherical particles, the specific solid-fluid interfacial surface area, a_{sf}, is given by the following equation [Nield and Bejan (1992)]:

$$a_{sf} = \frac{6(1-\varepsilon)}{d_p} \tag{10}$$

Initial and Boundary Conditions: The initial and boundary conditions which are needed to complete the mathematical models for the fluid flow and heat transfer in the rock-bed TES systems of interest are problem dependent. Thus, they will be elaborated later in this paper, with respect to the test and demonstration problems considered.

FINITE VOLUME METHOD

A finite volume method (FVM) was used to solve the mathematical models described in the previous section. It is an adaptation of a well-established FVM described in the works of Patankar (1980), and Baliga and Atabaki (2006). As full details of this FVM are available in the aforementioned references, only brief overviews of its key steps are presented here.

Domain Discretization: The Cartesian domains of interest are first discretized into contiguous rectangular control volumes that fill the domain exactly. Then, the nodes or grid points are located at the geometric centers of the control volumes, the centers of the control volume faces that coincide with the boundaries of the domain, and the corners of rectangular domain. The grid points or nodes lie on lines that are parallel to the coordinate axes, and these grid lines could be non-uniformly spaced. This domain discretization scheme is illustrated in Figure 2. All dependent variables are stored at the same set of nodes (co-located formulation). The thermophysical or effective properties that appear in the governing equations are also stored at the same set of nodes.

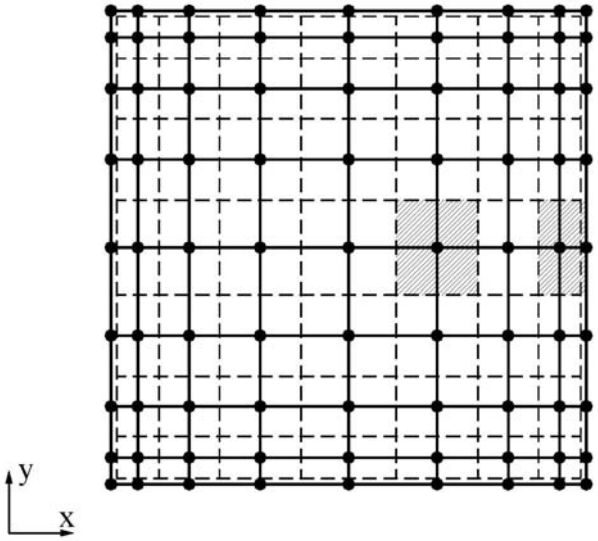

Figure 2: Discretization of a rectangular calculation domain: dashed lines indicate control volume faces; solid dots indicate nodes or grid points; solid lines denote grid lines; and the hashed regions show two control volumes, one in the domain interior and the other adjacent to its boundary.

Discretization of the Governing Equations: In the proposed FVM the governing differential equations are first integrated over the control volumes shown in Figure 2, and algebraic approximations to the integral conservation equations are then derived. These algebraic approximations are called the discretized equations. In the derivation of these discretized equations, the advection and diffusion terms are discretized using the hybrid scheme [Patankar (1980)], which is second-order accurate at low velocities (strictly, at grid Peclet number values less than 2) and uniform grids or geometrically expanding grids with relatively low expansion factors (as was the case in computer simulations of the rock-bed TES systems of interest); second-order quadratic interpolation is used at the boundaries, and appropriately adjusted to incorporate the specified boundary conditions [Baliga and Atabaki (2006)]; the reduced pressure is interpolated using piecewise-linear functions between the nodes; in the mass flow rate terms, the velocity components are interpolated using the so-called momentum interpolation scheme [Rhie and Chow (1983)], to avoid undesirable checkerboard pressure and velocity distributions that would otherwise afflict this equal-order co-located FVM [Patankar (1980)]; and the nodal values of thermophysical properties are interpolated to locations where the grid lines intersect the control-volume faces, using a resistance analogy (which reduces to the harmonic mean on uniform grids), as described in Patankar (1980). The fully-implicit scheme is used for the discretization in time.

Solution of the Discretized Equations: A sequential iterative variable adjustment procedure (SIVA) [Saabas and Baliga (1994); Baliga and Atabaki (2006)] was used to solve the nonlinear coupled sets of discretized equations for the steady-state nodal values of *u*, *v*, and *P*. These discretized equations were under-relaxed using an implicit scheme proposed by Patankar (1980), with the following under-relaxation factors: $\alpha_u = \alpha_v = 0.5$, and $\alpha_P = 1.0$. In each overall iteration of the SIVA scheme, decoupled and linearized sets of the discretized equations for each dependent variable of interest were solved iteratively using a line-Gauss-Seidel method. Full details of this method are available in the works of Patankar (1980), and Sebben and Baliga (1995). Overall convergence of the SIVA scheme was assumed to be achieved when suitably normalized absolute residues of the discretized equations for *u*, *v*, and *P* were all less than 10^{-4}.

For the computation of the unsteady nodal values of T_s and T_f, at each time step, the corresponding discretized equations were solved sequentially and iteratively, until the maximum values of suitably normalized absolute residues were all less than 10^{-4}. In each overall iteration of this sequential solution procedure, the linearized and decoupled set of discretized equations for each dependent variable (T_s and T_f) were again solved using an iterative line-Gauss-Seidel method.

TEST PROBLEMS

The applications of the proposed FVM to two test problems, the numerical results, and their comparisons to analytical solutions are concisely described in this section.

Test Problem 1: Fluid Flow in a Parallel-Plate Channel Filled with a Porous Medium

A schematic illustration of this test problem is given in Figure 3. It involves steady, two-dimensional, laminar fluid flow in a parallel-plate channel filled with an isotropic, homogeneous, porous medium made up of close-packed spherical particles of diameter d_p: L = 8.0 m, H = 0.5 m, and d_p = 0.0254 m, 0.0381 m, 0.0508 m, and 0.0635 m were considered.

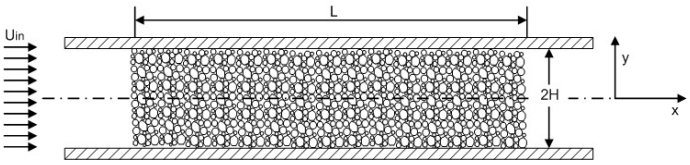

Figure 3: Fluid flow in a parallel-plate channel filled with a porous medium.

The fluid is Newtonian, with constant density and dynamic viscosity. The Forchheimer term is assumed to be negligibly small, thus C_F = 0. The fluid enters the porous region with a uniform velocity, u_{in}, and then flows through the channel in the porous region. Preliminary computations indicated that this fluid flow becomes fully developed within 5 – 10 particles diameters from the inlet plane. In the fully-developed region, $u = fnc(y)$ and $v = 0$.

Analytical solution in the fully-developed region: For the conditions described above, in the fully-developed region, Eq. (2), is automatically satisfied; the *y*-momentum equation reduces to $\partial P/\partial y$ = 0, which, in conjunction with the condition $u = fnc(y)$, leads to dP/dx = constant; and the *x*-momentum equation can be simplified and cast as follows:

$$\varepsilon\mu_f \frac{\partial^2 u}{\partial y^2} - \frac{\varepsilon^2 \mu_f}{K} u - \varepsilon^2 \frac{dP}{dx} = 0 \tag{11}$$

The boundary conditions on u are the following: at y = 0, $\partial u/\partial y$ = 0; and at $y = H$, u = 0.

The following dimensionless variables are introduced:

$$\eta = \frac{y}{H} \;;\; u^* = \frac{(\mu_f/\varepsilon)u}{(-dP/dx)H^2} \;;\; Da = \frac{K}{H^2} \;;\; \gamma = \frac{\varepsilon}{Da} \tag{12}$$

In this equation, *Da* is the Darcy number and ε is the porosity of the porous medium. Noting that the porous medium consists of close-packed spherical particles of uniform diameter d_p, the porosity was assigned a constant (average) value of ε = 0.40. The values of *K* were calculated using Carman-Kozeny relation given in Eq. (4).

Following Haji-Sheikh (2006), an analytical solution to this problem can be derived and cast in the following form:

$$\frac{u^*}{u^*_{av}} = \frac{u}{u_{av}} = \frac{\left[\cosh(\sqrt{\gamma}) - \cosh(\sqrt{\gamma}\eta)\right]}{\cosh(\sqrt{\gamma})\left[1 - \left\{\tanh(\sqrt{\gamma})/\sqrt{\gamma}\right\}\right]} \tag{13}$$

In this equation, u^*_{av} is the average value of u^* in the cross-section of the channel:

$$u^*_{av} = \int_0^1 u^* d\eta = u^*_{in} = \frac{(\mu_f/\varepsilon)u_{in}}{(-dP/dx)H^2} \tag{14}$$

The maximum value of u^* occurs at the center of the channel ($u^*_{\max} = u^*|_{\eta=0}$), and Eq. (13) can be recast as follows:

$$\frac{u^*}{u^*_{\max}} = \frac{u}{u_{\max}} = \frac{\left[\cosh(\sqrt{\gamma}) - \cosh(\sqrt{\gamma}\eta)\right]}{\left[\cosh(\sqrt{\gamma}) - 1\right]} \tag{15}$$

At this stage, a near-boundary region in the vicinity of the surface of the upper wall of the channel is defined as follows: $\eta_{edge,\,NB} \le \eta \le 1$, where $\eta_{edge,\,NB}$ is the value of η when $(u^*/u^*_{\max}) = (u/u_{\max}) =$ 0.99. Using Eq. (15), and introducing a term $\alpha = \left[0.01\cosh(\sqrt{\gamma}) + 0.99\right]$, it can be shown that

$$\eta_{edge,\,NB} = \ln\left[\alpha + \sqrt{\alpha^2 - 1}\right] \Big/ \sqrt{\gamma} \tag{16}$$

Here, it should be noted that $\alpha > 1$ in the problems of interest.

Numerical details, grid checks, and results: Again, the fluid flow becomes fully developed within a few particle diameters downstream from the inlet plane. Thus, though the proposed FVM was used to solve the full two-dimensional problem, that included the developing region, attention in this test problem was focused mainly on the fully-developed region.

Taking advantage of the symmetry surface at y = 0, the calculation domain was limited to $0 \le x \le L$ and $0 \le y \le H$. In the *x* direction, based on preliminary runs, a relatively modest grid of 20 uniform control volumes was found to be more than adequate, as attention was focused primarily on the fully developed region. In the *y* direction, the following domain discretization scheme was implemented: $N_{y,\,NB\,CVs}$ control volumes were uniformly distributed in the near-boundary region, $(\eta_{edge,\,NB}H) \le y \le H$, with $\eta_{edge,\,NB}$ calculated using Eq. (16); then, from $y = (\eta_{edge,\,NB}H)$ to y = 0, the control-volume extents were successively increased using a geometric expansion scheme, with a geometric factor GF = 1.05; the Δy value in the immediate vicinity of y = 0 was adjusted so that its lower face matched this location exactly, and, at the same time, its extent was not larger or smaller than 1.25 or 0.75 times, respectively, the previous value of Δy. Several different values of $N_{y,\,NB\,CVs}$ were tried and the corresponding numerical results in the fully-developed region were compared with those yielded by the analytical solution. The total number of grid

points in the x and y directions are indicated by $L1$ (= 22) and $M1$, respectively.

In the above-mentioned comparisons, the absolute values of the percentage differences between the analytical and numerical results in the fully-developed region, δ_J, were computed for each grid point J in the y direction as follows:

$$\delta_J = \left| \left[100 \text{ x} \left\{ \left(\frac{u}{u_{av}} \right)_{FVM} - \left(\frac{u}{u_{av}} \right)_{anal} \right\} \Big/ \left(\frac{u}{u_{av}} \right)_{anal} \right]_{I=L2,J} \right| \quad (17)$$

In this equation, $I = L2$ indicates grid points in the last set of control volumes in the x direction, immediately adjacent to the outlet plane at $x = L$, which was in the fully developed region for all cases considered in this test problem.

Table 1: Results for Test Problem 1: L = 8 m; and H = 0.5 m

d_p [m]	$L1$	$N_{y,\,NB\,CVs}$ = 10		$N_{y,\,NB\,CVs}$ = 20		$N_{y,\,NB\,CVs}$ = 40	
		$M1$	δ_{max}	$M1$	δ_{max}	$M1$	δ_{max}
0.0254	22	90	1.18	114	0.36	148	0.10
0.0381	22	81	1.18	105	0.36	139	0.10
0.0508	22	76	1.18	99	0.36	133	0.10
0.0635	22	71	1.18	95	0.37	129	0.11

It should be noted that for fixed values of H and u_{in}, the extent of the near-boundary region $(H - \eta_{edge,\,NB} H)$ increases as d_p increases; thus, with the geometrically expanding grid tied to the y-extent of the uniform control-volumes in the near-boundary region, $M1$ decreases as d_p increases, for a fixed value of $N_{y,\,NB\,CVs}$. The results in Table 1 show that for each combination of L, H, d_p, and $L1$, as the grid is refined in the y direction, with progressively increasing values of $N_{y,\,NB\,CVs}$ (= 10, 20, and 40), δ_{max} decreases monotonically, attesting to the consistency of the numerical solutions produced by the proposed FVM. For each of the four values of d_p considered, with $N_{y,\,NB\,CVs}$ = 20, the values of δ_{max} are all less than 0.37%. For the purposes of this project, this grid was considered to provide a good combination of computational costs and accuracy.

The FVM and analytical solutions show that for a fixed value of H and progressively smaller values of d_p (= 0.0254 m, 0.0381 m, and 0.0508 m), the (y/H)-extent of the near-boundary region reduces as (d_p/H) decreases. In the central portion of the channel cross-section, outside the near-boundary region, the superficial velocity profile is essentially uniform in the fully-developed region and one-dimensional (varying only with x) in the developing region. Advantage can be taken of these characteristics in computer-aided designs of rock-bed TES systems, by limiting the simulations to highly cost-effective one-dimensional simulations. This point will be elaborated further in the context of the demonstration problem presented in the next section.

Test Problem 2: Unsteady Heat Transfer in a Semi-Infinite Porous Medium with Uniform Fluid Velocity and a Step Change in Inlet Fluid Temperature

A schematic illustration of this test problem is given in Figure 4. It involves one-dimensional unsteady heat transfer in a semi-infinite porous medium, with uniform superficial fluid velocity ($u = u_{in}$ = constant throughout), and a step change in inlet fluid temperature, to a value greater than the initial temperature of the bed, $T_{in} > T_{ini}$.

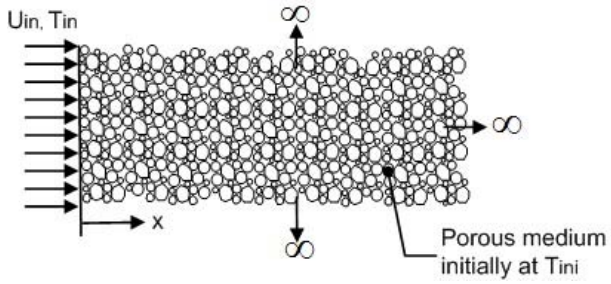

Figure 4: Unsteady heat transfer in a semi-infinite porous medium with uniform fluid velocity and a step change in inlet fluid temperature.

Following the analysis of Riaz (1977), attention in this test problem is limited to rock-bed TES systems in which the product of the interfacial heat transfer coefficient, h_{sf}, and the specific area, a_{sf}, between fluid and the solid particles is very large: thus, $T_f = T_s = T$. Furthermore, it is assumed that in the energy equation for the fluid, $\varepsilon(\rho c_P)_f (\partial T_f / \partial t)$ and $\partial(k_{f,eff} \partial T_f / \partial x)$ are negligible. Thus, Eqs. (5) and (6) can be simplified, added up (with $T_f = T_s = T$), and expressed as follows, along with the initial and boundary conditions:

$$(1-\varepsilon)(\rho c_P)_s \frac{\partial T}{\partial t} + \frac{\partial}{\partial x}\left[(\rho c_P)_f u T \right] = \frac{\partial}{\partial x}\left[(1-\varepsilon) k_s \frac{\partial T}{\partial x} \right] \quad (18)$$

$$T_{t=0} = T_{ini}$$

$$-(\partial T / \partial x)_{x=0} = \left(\frac{\left[\left(u \rho_f c_{p,f} \right) / \left\{ (1-\varepsilon) \rho_s c_{p,s} \right\} \right]}{\left[k_s / (\rho_s c_{p,s}) \right]} \right) (T_{in} - T)_{x=0} \quad (19)$$

$$(T)_{x \to \infty} = T_{ini}$$

Again following Riaz (1977), the following characteristic parameters and dimensionless variables are introduced:

$$v_{ch} = u(\rho c_p)_f / \left[(1-\varepsilon)(\rho c_p)_s \right] \; ; \; \alpha_s = k_s / (\rho c_p)_s$$
$$\tau = t / (\alpha_s / v_{ch}^2) \; ; \; \xi = x / (\alpha_s / v_{ch}) \; ; \; \Theta = (T - T_{ini}) / (T_{in} - T_{ini}) \quad (20)$$

In this equation, v_{ch} represents the reduced velocity of a purely advective thermal wave moving through the rock bed; α_s is the thermal diffusivity of the solid particles; (α_s / v_{ch}^2) is a characteristic time; and (α_s / v_{ch}) is a characteristic distance. Eqs. (18) and (19) are now recast as follows, respectively:

$$\frac{\partial \Theta}{\partial \tau} + \frac{\partial \Theta}{\partial \xi} = \frac{\partial^2 \Theta}{\partial \xi^2} \tag{21}$$

$$\Theta_{\tau=0} = 0 \ ; -(\partial \Theta / \partial \xi)_{\xi=0} = 1 - \Theta_{\xi=0} \ ; \ \Theta_{x \to \infty} = 0 \tag{22}$$

The analytical solution is the following [Riaz (1977)]:

$$\Theta = \frac{1}{2}\text{erfc}\left(\frac{\xi - \tau}{2\sqrt{\tau}}\right) + \sqrt{\frac{\tau}{\pi}}\exp\left\{-(\xi - \tau)^2 / (4\tau)\right\} - \frac{1}{2}(1 + \xi + \tau)\exp(\xi)\text{erfc}\left(\frac{\xi + \tau}{2\sqrt{\tau}}\right) \tag{23}$$

Numerical details, grid checks, and results: In this problem, the temperature distribution is unsteady and one-dimensional, and the extent of the domain is semi-infinite in the ξ direction. However, the proposed two-dimensional unsteady FVM was set up to as follows: $0 \le \xi \le 28$, with the boundary condition $(\partial \Theta / \partial \xi)_{\xi=28} = 0$; $0 \le (\zeta = y/(\alpha_s / u_{ch})) \le 0.4$, with the adiabatic boundary conditions $(\partial \Theta / \partial \zeta)_{\zeta=0} = (\partial \Theta / \partial \zeta)_{\zeta=0.4} = 0$; and $0 \le \tau \le 10$. Preliminary runs indicated that at $\tau =$ 10, the extent of the thermal penetration depth is well short of $\xi =$ 28, so the assumed the calculation domain is semi-infinite for all practical purposes.

In the ξ direction, $N_{\xi,\ NB\ CVs}$ control volumes were uniformly distributed in the near-boundary region, $0 \le \xi \le 1$; then, in the region $1 < \xi \le 28$, the control-volume extents were successively increased using a geometric expansion scheme, with a geometric factor GF = 1.05; the $\Delta\xi$ value in the immediate vicinity of ξ = 28 was adjusted so that its right face matched this location exactly, and, at the same time, its extent was not larger or smaller than 1.25 or 0.75 times, respectively, the previous value of $\Delta\xi$. In the dimensionless y direction, $(\zeta = y/(\alpha_s / u_{ch}))$, only two uniform control volumes, each with $\Delta\zeta =$ 0.2, were used; and this number was sufficient, as in this test problem, Θ does not change in the ζ direction. In the FVM simulations, three different values of $N_{\xi,\ NB\ CVs}$ (= 20, 40, and 100) and seven different values of the dimensionless time step, $\Delta\tau$, ranging from 1 x 10^{-4} to 0.1, were tried. The corresponding numerical results were compared to those yielded by the analytical solution given in Eq. (23).

In the above-mentioned comparisons, the absolute values of the percentage differences between the analytical and numerical results, normalized with respect to $\Theta = 1$, were computed for each grid point I in the ξ direction as follows:

$$\delta_I = \left| \left[(\Theta)_{FVM} - (\Theta)_{analytical} \right]_{I, J=2} \right| \text{ x } 100 \tag{24}$$

The values of $\delta_{\max} = (\delta_I)_{\max}$ at the dimensionless time $\tau = 0.1$ are presented in Table 2. In this table, $L1$, denotes the total number of grid points in the ξ direction (equal to the total number of control volumes in this direction plus two). In the ζ direction, the total number of grid point in that direction was constant at $M1 = (2 + 2) = 4$.

Table 2: Results for Test Problem 2 at $\tau = 0.1$

$\Delta\tau$	$N_{\xi,\ NB\ CVs}$ = 20		$N_{\xi,\ NB\ CVs}$ = 40		$N_{\xi,\ NB\ CVs}$ = 100	
	$L1$	$\delta_{\max}$	$L1$	$\delta_{\max}$	$L1$	$\delta_{\max}$
1x10^{-4}	91	0.55	124	0.28	203	0.12
2x10^{-4}	91	0.55	124	0.29	203	0.12
1x10^{-3}	91	0.59	124	0.32	203	0.16
2x10^{-3}	91	0.63	124	0.37	203	0.20
1x10^{-2}	91	0.98	124	0.71	203	0.55
2x10^{-2}	91	1.40	124	1.14	203	0.98
1x10^{-1}	91	4.48	124	4.25	203	4.11

The results in Table 2 show that as the dimensionless spatial grid and time step are refined, the maximum absolute percentage error, $\delta_{\max}$, decreases monotonically, attesting to the consistency of the numerical solution produced by the proposed FVM. For the combination $N_{\xi,\ NB\ CVs}$ = 40 ($L1$ = 124) and $\Delta\tau$ = 2 x 10^{-3}, the value of $\delta_{\max}$ is 0.37%. For the purposes of this project, this combination of dimensionless spatial grid and time step was considered to provide a good combination of computational costs and accuracy.

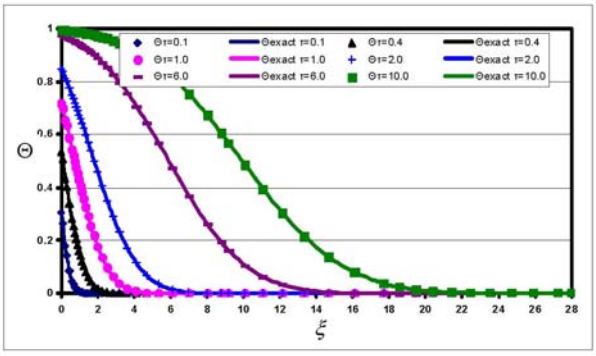

Figure 5: Numerical and exact distributions of Θ as a function of ξ for τ = 0.1, 0.4, 1.0, 2.0, 6.0, and 10.0: the results displayed in this figure were computed with the combination $N_{\xi,\ NB\ CVs}$ = 40 ($L1$ = 124) and $\Delta\tau$ = 2 x 10^{-3}.

A graphical representation of the numerical and analytical results for Θ as a function of ξ are shown in Figure 5 for τ = 0.1, 0.4, 1.0, 2.0, 6.0, and 10.0: the results displayed in this figure were computed with the combination $N_{\xi,\ NB\ CVs}$ = 40 ($L1$ = 124) and $\Delta\tau$ = 2 x 10^{-3}. These results show excellent agreement between the numerical and analytical results (as was discussed earlier, $\delta_{\max}$ = 0.37%).

DEMONSTRATION PROBLEM

A schematic illustration of this demonstration problem is given in Figure 6. It involves a parallel-plate channel filled with close-packed rocks of essentially spherical shape and uniform diameter, d_p. The plates are impermeable and separated by a perpendicular distance *2H*.

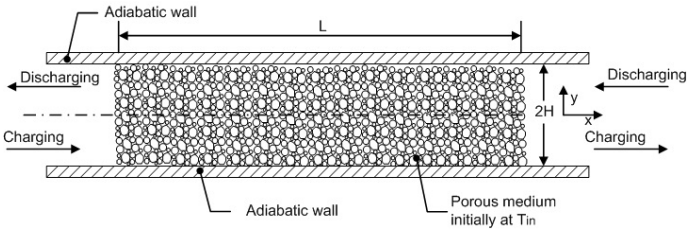

Figure 6: Schematic illustration of the demonstration problem.

The rock bed is made of granite, as it is inexpensive, thermally stable, and widely available. Air is used for the charging and discharging operations. The thermophysical properties of this granite and air are given in Tables 3 and 4.

Table 3: Thermophysical properties of granite (T_{av} = 30 ^{o}C) [Incropera and DeWitt (2002)]

ρ [kg/m^3]	c_P [J/kg·K]	k [W/m.K]
2630	775	2.79

Table 4: Thermophysical properties of air (T_{av} = 30 ^{o}C ; p = 1 std atm) [Incropera and DeWitt (2002)]

ρ [kg/m^3]	c_P [J/kg·K]	k [W/m·K]	μ [kg/m·s]
1.08	1008	0.028	2.20 x 10^{-5}

The porosity of the rock bed (close-packed spherical particles of granite) is assigned the constant value of $\varepsilon = 0.40$. The volume and depth of the rock bed are fixed at V = 80 m^3 and W = 10 m, respectively. Three combinations of L and H are considered: L = 8 m and H = 0.5 m; L = 6 m and H = 2/3 m; and L = 4 m and H = 1 m. For each of these combinations, four different particle diameters are investigated: d_p = 0.0254 m, 0.0381 m, 0.0508 m, and 0.0635 m.

During the charging operation, the air enters the rock bed with a uniform velocity, $u_{in,ch}$, on its left side, develops as it flows through it from the left to the right, and exits on its right side; and during the discharging operation, the air enters the rock bed with a uniform velocity, $u_{in,disch}$, on its right side, develops as it flows through it from the right to the left, and exits on its left side. In both the charging and discharging operations, the volume flow rate of the air is maintained constant at Q_{air} = $Q_{air,ch}$ = $Q_{air,disch}$ = 1 m^3/s. Thus, $u_{in,ch} = Q_{air,ch}/(2WH)$, $v_{in,\ ch} = 0$, $u_{in,\ disch} = -Q_{air,ch}/(2WH)$, and $v_{in,disch} = 0$. At the top and bottom walls of the channel, the air velocity (superficial) is assigned the value of zero (no-slip and impermeability conditions); and at the outlet plane, in both the charging and discharging operations, the viscous transport of momentum is assumed to be negligible compared to its advection transport, which corresponds to the well-established outflow boundary treatment [Patankar (1980)].

The intrinsic-phase-average temperature of the air (T_f) at the inlet plane during the charging and discharging operations was maintained constant at $T_{f,ch,in}$ = 50 ^{o}C and $T_{f,disch,inlet}$ = 10 ^{o}C, respectively. Initially, the rock bed and the air inside it are assigned a uniform temperature of $T_{s,\ ini}$ = $T_{f,\ ini}$ = T_{ini} = 30 ^{o}C. With respect to the intrinsic-phase-average temperature of the air, T_f, at the outlet plane, in both the charging and discharging operations, the conduction transport of thermal energy is assumed to be negligible compared to its advection transport, again following the outflow boundary treatment [Patankar (1980)]. The top and bottom walls of the channel are assumed to be adiabatic in this demonstration problem, with respect to both T_s and T_f, mainly to concentrate attention on the storage aspects of the rock bed, rather than the rates of heat loss from it to the ambient (which, in practice, would be negligible compared to the rates of charging and discharging of thermal energy to and from the rock bed, if it is well insulated). In the same spirit, with respect to the intrinsic-phase-average temperature of the rock bed, T_s, the inlet and exit planes of the rock bed are also assumed to be essentially adiabatic.

In this demonstration problem, the durations of the charging and discharging operations, t_{ch} and t_{disch}, respectively, are each 12 hours, and follow one another. For the above-mentioned conditions, with repeated charging and discharging cycles, the intrinsic-phased-average temperature of the rock bed, and also its thermal energy storage and harvesting characteristics, take on a time-periodic behavior. Based on preliminary computer simulations, using the FVM described earlier, it was established that the aforementioned time-periodic behavior is well established when the number of charging-discharging cycles ($N_{ch+disch}$) reaches a value between 5 and 10. Thus, the final simulations were conducted with $(N_{ch+disch})_{total}$ = 13, for each of the 12 cases investigated: the three

combinations of L and H (L = 8 m and H = 0.5 m; L = 6 m and H = 2/3 m; and L = 4 m and H = 1 m); and for each of these three combinations, four values of particle diameter: d_p = 0.0254 m, 0.0381 m, 0.0508 m, and 0.0635 m.

The air flow rates and inlet conditions used in this demonstration problem correspond to a rough (first design pass) model of a solar energy application with the following characteristics: 100 flat-plate collectors, each with an effective area of 1 m x 1m; average solar irradiation of 500 W/m^2; collector efficiency of 50%; and average air temperature increase of 25 ^{o}C as it flows through the collector. The rock (granite) bed volume used in this problem is roughly 2.5 times the minimum volume that is needed to sensibly store the full amount of collected solar thermal energy with a rock-bed temperature increase of 40 ^{o}C.

Performance indicators: The performance of the rock-bed thermal energy storage system considered in this demonstration problem is assessed with respect to two key indicators, namely, an efficiency coefficient, η, and a coefficient of performance, COP. For each charging period, t_{ch}, the efficiency coefficient, η_{ch}, is the total thermal energy stored, E_{ch}, divided by the maximum thermal energy that could have been stored; and for each discharging period, t_{disch}, the efficiency coefficient, η_{disch}, is the total thermal energy harvested, E_{disch}, divided by the maximum thermal energy that could have been harvested. Thus,

$$\eta_{ch} = \frac{E_{ch}}{Q_{air,ch}\left(\rho c_P\right)_f \left(T_{ch} - T_{disch}\right) t_{ch}} \tag{25}$$

$$\eta_{disch} = \frac{E_{disch}}{Q_{air,disch}\left(\rho c_P\right)_f \left(T_{ch} - T_{disch}\right) t_{disch}} \tag{26}$$

$$E_{ch} = \sum_{\substack{n=1,nch \\ charging}} \left[\sum_{\substack{I,J \\ Vol\ Bed}} \left(1-\varepsilon\right)\left(\rho c_P\right)_s \left(T_s - T_s^o\right)_{I,J} \left(\Delta x\right)_I \left(\Delta y\right)_J W \right]_n$$

$$E_{disch} = \sum_{\substack{n=1,ndisch \\ discharging}} \left[\sum_{\substack{I,J \\ Vol\ Bed}} \left(1-\varepsilon\right)\left(\rho c_P\right)_s \left(T_s^o - T_s\right)_{I,J} \left(\Delta x\right)_I \left(\Delta y\right)_J W \right]_n \tag{27}$$

In Eq. (27), I and J are the indices of the grid point in each of the control volumes into which the calculation domain is discretized; Δx and Δy are the x- and y-extents of the control volumes; W is the width of the rock bed (= 10 m in this demonstration problem); *nch* and *ndisch* are the total number of time steps in each charging and discharging operations, respectively; $(T_s)_{I,J}$ is the intrinsic-phase-average temperature of the rock bed at the grid point (I,J) at the *end* of time-step n; and $(T_s^o)_{I,J}$ is the intrinsic-phase-average temperature of the rock bed at the grid point (I,J) at the *start* of time-step n.

For each charging period, t_{ch}, the coefficient of performance, COP_{ch}, is the total thermal energy stored, E_{ch}, divided by the total pumping work that is needed to push the air through the rock bed; and for each discharging period, t_{disch}, the coefficient of performance, COP_{disch}, is the total thermal energy harvested, E_{disch}, divided by the total pumping work that is needed to push the air through the rock bed. Thus,

$$COP_{ch} = \left[E_{ch} \Big/ \left\{ \left(Pumping\ \ Power \right)_{ch} t_{ch} \right\} \right]$$
$$COP_{disch} = \left[E_{disch} \Big/ \left\{ \left(Pumping\ \ Power \right)_{disch} t_{disch} \right\} \right] \tag{28}$$

Numerical details: Making use of the symmetry surface at $y = H$ (see Figure 6), only the bottom-half of the channel was included in the calculation domain: $0 \le x \le L$ and $0 \le y \le H$. In the y direction, $N_{y,\ NB\ CVs}$ control volumes were uniformly distributed in the region $0 \le y \le \left\{(1-\eta_{edge,\ NB})H\right\}$, with $\eta_{edge,\ NB}$ calculated using Eq. (16); then, from $y = \left\{(1-\eta_{edge,\ NB})H\right\}$ to y = H, the control-volume extents were successively increased using a geometric expansion scheme, with a geometric factor GF = 1.05; if in this geometric expansion scheme, $\Delta y \ge H/40$, then it was fixed at this value (H/40); the Δy value in the immediate vicinity of $y = H$ was adjusted so that its upper face matched this location exactly, and its extent was not larger or smaller than 1.25 or 0.75 times, respectively, the previous value of Δy. Based on the results of Test Problem 1, $N_{y,\ NB\ CVs}$ = 20 was used in this demonstration problem.

In the x direction, based on the results of Test Problem 2, the following grid was implemented and used during both the charging and discharging operations: $N_{x,\ NB\ CVs}$ = 20 control volumes were uniformly distributed in a near-boundary region, $0 \le x \le \lambda_2$; then, in the region $\lambda_2 < x \le L/2$, the control-volume extents were successively increased using a geometric expansion scheme, with a geometric factor GF = 1.05; if in this geometric expansion scheme, $\Delta x \ge L/80$, then it was fixed at this value (L/80); the Δx value in the immediate vicinity of x = L/2 was adjusted so that its right face matched this location exactly, and its extent was not larger or smaller than 1.25 or 0.75 times, respectively, the previous value of Δx; and finally, a mirror reflection of the grid in the region $0 \le x \le L/2$ was used to discretize the calculation domain in the region $L/2 \le x \le L$. In this grid design, following Riaz (1977), the extent of the near-boundary region, λ_2, was calculated according to the following equation:

$$\lambda_2 = (u_{inlet}\rho_f c_{p,f})/(a_{sf} h_{sf}) \tag{29}$$

The solid-fluid interfacial heat transfer coefficient, h_{sf}, and specific area, a_{sf}, were calculated using Eqs. (8) to (10).

Based on the results of Test Problem 2, the time step in this demonstration problem was chosen in accordance with the

following scheme: in the time period $0 \le t \le t_{characteristic}$, 500 uniform time steps were employed; then the time steps were successively increased using a geometric expansion scheme, with a geometric factor GF = 1.05; if in this geometric expansion scheme, $\Delta t \ge t_{ch}/144$ (note $t_{ch} = t_{disch} =$ 43,200 s), then it was fixed at this value ($t_{ch}/144$); and the Δt value in the immediate vicinity of $t = N_{ch+disch} t_{ch}$ (again, note that here, $t_{ch} = t_{disch} =$ 43,200 s) was adjusted to fit this time exactly, while ensuring that its extent was not larger or smaller than 1.25 or 0.75 times, respectively, the previous value of Δt. The characteristic time, $t_{characteristic}$, was computed using the following equation [Riaz (1977)]:

$$t_{characteristic} = (1-\varepsilon)\rho_s c_{p,s}/(a_{sf} h_{sf}) \quad (30)$$

As was discussed earlier, when the value of u_{in} and also the outflow condition are maintained uniform throughout the charging operation (as is the case in this demonstration problem), the distribution of the superficial fluid velocity within the rock bed may be assumed to be essentially steady. A similar statement also applies to the discharging operation. Thus, for each case considered, at the start of the simulations, the steady-state distributions of the superficial velocity components, *u* and *v*, were computed and stored for both the charging and discharging arrangements. These stored distributions of *u* and *v* were then used repeatedly during the successive charging and discharging operations.

Results: The variations with time of the intrinsic-phase-average temperature of the rock bed, T_s, at three specific points corresponding to $y = H$ and $x = 0$, $L/2$ (roughly), and L are plotted in Figure 7, for the case in which L = 6 m, H = 2/3 m, and d_p = 0.0254 m. These results clearly show that for $N_{ch+disch} \ge 5$, T_s varies periodically with t, for all practical purposes. Similar results were obtained for all other combinations of *L*, *H*, and d_p considered in this demonstration problem.

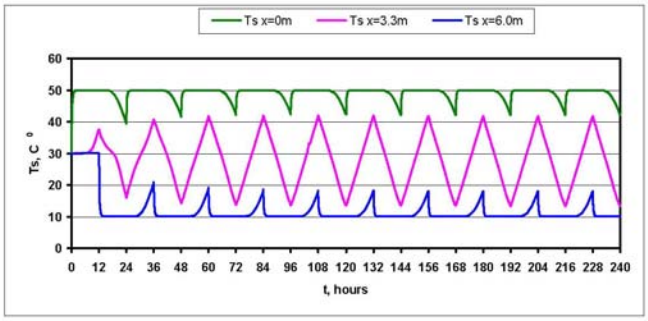

Figure 7: Variations with time of T_s at three specific points corresponding to $y = H$ and $x = 0$, $L/2$ (roughly), and L, for L = 6 m, H = 2/3 m, and d_p = 0.0254 m.

Results for E_{ch}, η_{ch}, and COP_{ch} at the end of the tenth charging-discharging cycle ($N_{ch+disch} = 10$), when the rock bed is in its time-periodic behavior, are presented in Table 5 for all 12 cases considered in this Demonstration Problem. These results indicate that the η_{ch} (which equals η_{disch} in the time-periodic regime of this rock bed) is greater than 90% for the cases considered, and attains its highest value (η_{ch} = 95.9%) for the combination L = 8 m, H = 0.5 m, and d_p = 0.0254 m. The values of COP_{ch} (which equals COP_{disch} in the time-periodic regime of this rock bed) are all greater than 500, and attains the high (but not the highest) value of 503.2 for the combination L = 8 m, H = 0.5 m, and d_p = 0.0254 m. Therefore, this is the recommended combination if the selection criteria demand the highest value of η_{ch} with a reasonably high value of COP_{ch}. However, if the selection criteria require the highest value of COP_{ch} along with a reasonably high value of η_{ch}, then the recommended combination is L = 4 m, H = 1 m, and d_p = 0.0635 m, for which η_{ch} = 90.6% and COP_{ch} = 10027.72.

Table 5: Results for the Demonstration Problem

L [m]	d_p [m]	E_{ch} [MJ]	η_{ch}	COP_{ch}	$COP_{1D,}$ ch	Δ_{1D-2D}
4	0.0254	1908.9	0.942	3135.1	3135.4	0.010
	0.0381	1887.7	0.932	5394.8	5400.4	0.104
	0.0508	1862.6	0.919	7714.4	7727.5	0.169
	0.0635	1835.9	0.906	10027.7	10046.5	0.188
6	0.0254	1933.9	0.954	1091.8	1092.2	0.034
	0.0381	1915.2	0.945	1815.4	1818.4	0.161
	0.0508	1893.7	0.935	2545.1	2550.4	0.208
	0.0635	1870.9	0.923	3267.0	3275.4	0.257
8	0.0254	1943.8	0.959	503.2	502.9	0.063
	0.0381	1927.7	0.951	819.6	821.2	0.191
	0.0508	1908.7	0.942	1135.8	1138.7	0.254
	0.0635	1889.3	0.932	1448.5	1452.9	0.307

Also presented in Table 5, are the results for $COP_{1D,\,ch}$ (obtained by assuming that both the fluid flow and heat transfer inside the rock-bed TES system employed in this demonstration problem are essentially one-dimensional) and Δ_{1D-2D}, which is the absolute value of the *percentage* difference between the values of COP_{ch} (obtained with the two-dimensional simulations) and $COP_{1D,\,ch}$. The values of Δ_{1D-2D} are all less

than 0.31%. These results show clearly that the one-dimensional simulations are a very cost-effective tool for the thermofluid design optimization of this rock-bed TES system.

CONCLUSION

The main contributions of this work are the following: proposal of cost-effective mathematical models of fluid flow and heat transfer in rock beds; adaptation of a finite volume method (FVM) for the solution of this model; applications of this FVM to two test problems (with analytical solutions) and one demonstration problem; proposal of suitable thermofluid performance evaluation criteria for the rock-bed TES systems of interest; and presentation and discussions of the results. Energy storage efficiencies and coefficients of performance were proposed as suitable thermofluid performance indicators for these systems. The results of the test problems showed that the proposed FVM produces consistent and accurate solutions. The results of the demonstration problem show how the proposed mathematical models and FVM can be used to study and optimize the performance of rock bed storage systems. The results of the demonstration problem were also used to show that simple one-dimensional unsteady models of the fluid flow and heat transfer in the rock-bed TES systems of interest would be adequate and very cost-effective for computational optimization of their thermofluid design.

ACKNOWLEDGMENTS

Financial sponsorship of this work by the Natural Sciences and Engineering Research Council (NSERC) of Canada, through research grants to the third author, is gratefully acknowledged.

REFERENCES

Alazmi, B. and Vafai, K. (2000), Analysis of Variants within the Porous Media Transport Models, *ASME J. Heat Transfer*, **122**, pp. 303-326.

Baliga, B.R. and Atabaki, N. (2006), Control-Volume-Based Finite Difference and Finite Element Methods, in *Handbook of Numerical Heat Transfer, 2nd Ed.*, W.J. Minkowycz, E.M. Sparrow, and J.Y. Murthy (Editors), Chapter 6, John Wiley & Sons, New York.

Brinkman, H. C. (1947), A Calculation of the Viscous Force Exerted by a Flowing Fluid on a Dense Swarm of Particles, Applied Scientific Research, **A1**, 27-34.

Darcy, H. P. C. (1856), *Les Fontaines Publiques de la Ville de Dijon*, Victor Dalmont, Paris.

Dincer, I. and Rosen, M. A. (2002), *Thermal Energy Storage: Systems and Applications*, John Wiley, New York.

Dullien, F. A. L. (1992), *Porous Media: Fluid Transport and Pore Structure*, 2nd Ed., Academic Press, San Diego.

Haji-Sheikh, A. (2006), Fully Developed Heat Transfer to Fluid Flow in Rectangular Passages Filled with Porous Materials, *ASME J. Heat Transfer*, **128**, 550-556.

Incropera, F. P. and DeWitt, D. P. (2002), *Fundamentals of Heat and Mass Transfer*, 5th Ed., John Wiley, New York.

Kaviany, M. (1995), *Principles of Heat Transfer in Porous Media*, Springer-Verlag, New York.

Mehling, H. and Cabeza, L.F. (2008), *Heat and Cold Storage with PCM: An Up to Date Introduction into Basics and Applications*, Springer, Berlin, Germany.

Nield, D. A. and Bejan, A. (1999), *Convection in Porous Media*, 2nd Ed. Springer-Verlag, New York.

Paksoy, H.O. (2007), *Thermal Energy Storage for Sustainable Energy Consumption: Fundamentals, Cases Studies and Design*, Springer, Dordrecht, The Netherlands.

Patankar, S.V. (1980), *Numerical Heat Transfer and Fluid Flow*, Hemisphere/McGraw-Hill, New York.

Rhie, C.M. and Chow, W.L. (1983), Numerical Study of the Turbulent Flow Past an Airfoil with Trailing Edge Separation, *AIAA Journal*, **21**, 1525-1532.

Riaz, M. (1977), Analytical Solutions for Single and Two-Phase Model of Packed Bed Thermal Storage Systems, ASME J. Heat Transfer, **99**, 489-492.

Rosen, M. A. (1992), Appropriate Thermodynamic Performance Measures for Closed Systems for Thermal Energy Storage, *J. Solar Energy Engineering*, **114**, 100-105.

Saabas, H.J. and Baliga, B.R. (1994), A Co-Located Equal-Order Control-Volume Finite Element Method for Multidimensional, Incompressible Fluid Flow – Part I: Formulation, *Num. Heat Transfer, Part B*, Vol. 26, pp. 381-407.

Scheidegger, A. E. (1974), *The Physics of Flow Through Porous Media*, 3rd Ed., University of Toronto Press, Toronto.

Schumann, T. E. W. (1929), Heat Transfer: A Liquid Flowing through a Porous Prism, *J. Franklin Institute*, **208**, 405-416.

Sebben, S. and Baliga, B.R. (1995), Some Extensions of Tridiagonal and Pentadiagonal Matrix Algorithms, *Num. Heat Transfer, Part B*, Vol. 28, pp. 323-351.

Vafai, K. and Tien, C.L. (1981), Boundary and Inertia Effects on Flow and Heat Transfer in Porous Media, *Int. J. Heat Mass Transfer*, **24**, 195-203.

Wakao, N. and Kaguei, S. (1982), *Heat and Mass Transfer in Packed Beds*, Gordon and Breach, New York.

Whitaker, S. (1996), The Forchheimer Equation: A Theoretical Development, *Transport in Porous Media*, **25**, 26-61.

Whitaker, S. (1999), *The Method of Volume Averaging*, Kluwer, Dordrecht, The Netherlands.

White, F.M. (1991), *Viscous Fluid Flow*, 2nd Ed., McGraw-Hill, New York.

Zalba, B., Marin, J.M., Cabeza, L.F., and Mehling, H. (2003), Review on Thermal Energy Storage with Phase Change: Materials, Heat Transfer Analysis and Applications, *Applied Thermal Engineering*, **23**, 251-283.

